

Bias and variance reduction and denoising for CTF Estimationⁱ

Ayelet Heimowitz, Joakim Andén, and Amit Singer

Abstract—When using an electron microscope for imaging of particles embedded in vitreous ice, the objective lens will inevitably corrupt the projection images. This corruption manifests as a band-pass filter on the micrograph. In addition, it causes the phase of several frequency bands to be flipped and distorts frequency bands. As a precursor to compensating for this distortion, the corrupting point spread function, which is termed the contrast transfer function (CTF) in reciprocal space, must be estimated. In this paper, we will present a novel method for CTF estimation. Our method is based on the multi-taper method for power spectral density estimation, which aims to reduce the bias and variance of the estimator. Furthermore, we use known properties of the CTF and of the background of the power spectrum to increase the accuracy of our estimation. We will show that the resulting estimates capture the zero-crossings of the CTF in the low-mid frequency range

Index Terms—keywords

I. INTRODUCTION

In recent years, single particle cryo-electron microscopy (cryo-EM) has emerged as a leading tool for resolving the 3D structure of macromolecules from multiple 2D projections of a specimen. In this technique, multiple occurrences of the sought-after particle are embedded in vitreous ice and imaged in an electron microscope. The output of this imaging process is a set of micrographs, each containing multiple 2D projections of the specimen, where each projection is associated with some unknown location and orientation.

The micrograph does not contain clean projections of the specimen, but is contaminated by several factors such as noise, stemming from an inherent limitation on the number of imaging electrons that can be applied to the specimen, ice aggregates, carbon film projection and convolution with a point spread function. The point spread function (PSF) originates in the electron microscope, and causes three types

of distortion in the micrograph. First, the PSF acts as a band-pass filter on the micrograph. Second, it causes the phase of several frequency bands to be flipped. Lastly, even the frequency bands that are not filtered out are distorted. In order to compensate for this, the point spread function must be estimated.

The task of estimating the point spread function is one of the initial objectives in the single particle cryo-electron microscopy pipeline. It is necessary since low resolution projection images will lead to a low resolution reconstruction. Indeed, PSF correction is useful for a variety of tasks in the cryo-EM pipeline, such as particle picking [?], class averaging, ab initio reconstruction, refinement and heterogeneity analysis.

Since the PSF acts as a convolutional operator on the clean projections, it is convenient to estimate its Fourier transform, known as the contrast transfer function (CTF). In this way, the Fourier transform of the projections are multiplied by the CTF, which is an oscillatory function, with values ranging from -1 to 1 . This multiplication causes Thon rings [1] to appear in the power spectrum of the micrograph. Therefore, in order to estimate the CTF, it is common practice to estimate the power spectrum.

The CTF is typically modeled as a sine function whose argument depends on the spatial frequency and several parameters of the objective lens of the micrograph. The most important parameters are the defocus and astigmatism of the objective lens. Other parameters are the electron wavelength (which depends on the voltage of the electron gun), the spherical aberration of the objective lens, and the amplitude contrast. Estimating the CTF is done by estimating the defocus and astigmatism, since the other parameters are typically fixed.

Fitting the Thon rings to the CTF model is complicated by the high levels of noise present in the micrograph. Each micrograph has a very low signal-to-noise ratio (SNR) due to the inherent limitation on electron dose required to avoid radiation damage to the specimen. The power spectrum of the micrograph is typically modeled as the sum of a term

A. Heimowitz is with the Program in Applied and Computational Mathematics, Princeton University, Princeton, NJ e-mail: aheimowitz@math.princeton.edu

J. Andén is with the Center for Computational Mathematics, Flatiron Institute, New York, NY

A. Singer is with the Program in Applied and Computational Mathematics and the Department of Mathematics, Princeton University, Princeton, NJ

that depends on the squared CTF with the power spectrum of the noise. The noise power spectrum, referred to as the background, will somewhat mask the Thon rings, causing a slight shift to the minima and maxima of the squared CTF.

In order to compensate for this shift, the background term must be estimated and subtracted from the micrograph power spectrum. One method of estimation models the background as a Gaussian, and fits the local minimas of the 1D radial profile of the power spectrum to this model [2]. The idea here is that at the minima of the power spectrum, the contribution from the squared CTF term should be approximately 0, and therefore those specific frequencies are dominated by the background. Another method for background estimation is through a low-pass filtering of the power spectrum of the micrograph [3].

Assuming that the power spectrum of the micrograph and the background were both estimated perfectly, the background-subtracted power spectrum only consists of the squared CTF term. If it were possible to compute the correlation between the background-subtracted power spectrum and the square of simulated CTFs with each possible combination of defocus and astigmatism, the maximal correlation would correspond with the sought-after defocus and astigmatism. As this is not feasible, a search over the parameter space is often employed [4], [3], [5], [6]. This is followed by gradient descent optimization to find the true correlation maximum.

Other approaches use least-squares to fit the minima of the power spectrum to the zeros of the CTF model [2], or to identify a single ring of zero crossings as an indicator for astigmatism, and derive a closed-form solution of the CTF parameters [7]. Regardless of the CTF estimation method, estimating the background-subtracted power spectrum is necessary. In this paper we present a novel approach to this task. We show that our approach leads to an estimate where the zero-crossings of the Thon rings can be easily obtained in the low-to-mid spatial frequencies.

The first step of our method is estimating the power spectral density of the micrograph. There are two main approaches for this estimation. The first approach is periodogram-based, and is used in, for example, [4], [3], [5]. The second approach is parametric estimation methods [8]. The vast majority of methods adopt the periodogram for power spectrum estimation due to its speed and simplicity. However, the periodogram estimator produces a biased and inconsistent estimate of the micrograph power spectrum.

We estimate the power spectrum using a modified periodogram estimate [9]. We reduce the variance of the periodogram estimator using Welch's method [10]. In addition, we reduce the bias of this estimator through use of data

tapers [11]. We further reduce the variance of the estimator by averaging over multiple tapers [12].

Next, we turn to the effects of noise on the power spectrum estimation. The power spectrum of the micrograph is commonly modeled as the sum of the data power spectrum convolved with the PSF and the noise power spectrum. This second term, called the background spectrum, is known to be a well-behaved, monotonically decreasing function.

As the background can mask some of the Thon rings, it is good practice to estimate and remove it from the micrograph power spectrum []. Otherwise, the background term can lead to errors when fitting the Thon rings to CTF model. In this paper, we present a novel method based on linear programming (LP) for estimating the noise power spectrum.

The last phase of our power spectral density estimator is geared towards removing any additional background noise not accounted for by our LP background estimation. Since the CTF is supported on a limited number of steerable basis functions, we project the background-subtracted PSD onto the space determined by these functions. Since this will remove only content that could not be due to the CTF, it can be considered as a denoising process that improves the estimation of the power spectrum.

We present two solutions to the CTF estimation problem. Our first solution is similar to [4], [3], [5], where the estimation is done according to the maximum of correlation with synthetic CTFs. We use our background-subtracted power spectrum for this cross-correlation function. Our second solution uses the spatial frequencies of the zero-crossings of the estimated background-subtracted PSD to define an overdetermined system of equations over the CTF parameters.

Our method is experimentally verified in Section ?? . We compare the correlation of our estimation with that of the estimation of [3], [5] on several datasets, including the CTF challenge [13].

II. MATERIAL AND METHODS

A. The contrast transfer function

The formation model for projection images procured by an electron-microscope can be expressed, under the weak phase object approximation, by the following linear model [4], [14], [15], [1],

$$y = h * x + b. \quad (1)$$

Here y is an observed projection image (or, equivalently, a micrograph or frame), x is the clean projection, b is noise and h is a point spread function which distorts the projection image. In reciprocal space, this model can be expressed as

$$Y = H \cdot X + B, \quad (2)$$

where H is known as the *contrast transfer function* (CTF).

In order to achieve high resolution reconstructions, the distortion introduced by the CTF should be corrected. It is therefore important to reliably estimate the unknown parameters of the CTF. To this end, we examine the theoretical model of the CTF [3]

$$H(\mathbf{g}) = -\sin(\chi(\mathbf{g}, \Delta f, Cs, \lambda, w)), \quad (3)$$

where \mathbf{g} is the spatial frequency, and

$$\chi(\mathbf{g}, \Delta f, Cs, \lambda, w) = \frac{1}{2}\pi\lambda|\mathbf{g}|^2\Delta f - \frac{1}{2}\pi\lambda^3|\mathbf{g}|^4Cs + w. \quad (4)$$

Many CTF estimation approaches assume the amplitude contrast w , the spherical aberration Cs and the electron wavelength λ are known, and therefore focus on estimating the defocus of the objective lens Δf . The defocus itself is determined by three unknown parameters,

$$\Delta f = \Delta f_1 + \Delta f_2 + (\Delta f_1 - \Delta f_2) \cos(2[\alpha_g - \alpha_f]), \quad (5)$$

where $\mathbf{g} = (|\mathbf{g}|, \alpha_g)$ are the polar coordinates of the spatial frequency and $(\Delta f_1 - \Delta f_2)$ is the astigmatism of the objective lens, with α_f being the angle between Δf_1 and the x-axis.

We conclude from (3) that the value of H oscillates between -1 and 1 . When the astigmatism is fully corrected, i.e. $\Delta f_1 = \Delta f_2$, then the CTF is radially symmetric. In an astigmatic image with $Cs = 0$, the CTF is made of ellipses, centered at the origin ($\mathbf{g} = [0 \ 0]^T$). All pixels on a single ellipse have the same CTF value. The spherical aberration accounts for small variations from the elliptical shape.

In order to estimate the CTF parameters, we consider the power spectral densities of the y , which can be expressed as the sum of two power spectra [2], [16],

$$PSD_y(u, v) = |H(u, v)|^2 PSD_x(u, v) + PSD_b(u, v), \quad (6)$$

where PSD_x is the power spectrum of the true particle projections and PSD_b is the power spectrum of noise, and is commonly referred to as the background. Often PSD_x is considered to be a constant in the relevant spatial frequencies [2]. Therefore, $PSD_y(\mathbf{g}) - PSD_b(\mathbf{g})$ is proportional to $|H(u, v)|^2$, and the CTF can be estimated by cross-correlation of the background subtracted power spectrum with the square of simulated CTF functions. This estimation method was used, e.g. in [4], [3], [5].

On the other hand, if PSD_x is not approximately constant, the power spectrum can be estimated from the zero-crossings of the background subtracted power spectrum. That is, for spatial frequencies where $H(\mathbf{g}) = 0$, it must be the case that $PSD_y(\mathbf{g}) - PSD_b(\mathbf{g}) = 0$. Therefore, matching the

zero-crossings of the background-subtracted power spectrum will reveal the parameters of the CTF.

We conclude that the first step in CTF estimation should be estimating the power spectrum of the micrograph. In Sections II-B-?? we propose a method for this estimation. We show that, using this method, the zero-crossings of the CTF can be identified.

B. Power Spectral Densities

Popular due to its speed and ease of implementation, the periodogram is often used to estimate the power or amplitude spectrum of experimental data. For micrograph \mathbf{y} of size $M \times N$, the periodogram estimate of the power spectrum, S_P , is

$$S_P(u, v) = \frac{1}{MN} \left| \sum_{m=0}^{M-1} \sum_{n=0}^{N-1} y[m, n] e^{-j2\pi(\frac{um}{M} + \frac{vn}{N})} \right|^2. \quad (7)$$

and the periodogram estimate of the amplitude spectrum, A_P , is

$$A_P(u, v) = \frac{1}{MN} \left| \sum_{m=0}^{M-1} \sum_{n=0}^{N-1} y[m, n] e^{-j2\pi(\frac{um}{M} + \frac{vn}{N})} \right|. \quad (8)$$

We note that as

$$\frac{1}{MN} S_P(u, v) = A_P(u, v)^2, \quad (9)$$

the estimate of the amplitude spectrum can be computed from the estimate of the power spectrum in linear time, and vice versa.

There are two main drawbacks to this method of power spectral density (PSD) estimation. First, while the periodogram is asymptotically unbiased [12], a micrograph does not have enough samples (pixels) available to produce a sufficiently unbiased estimation [11]. The second drawback is that the periodogram is an inconsistent estimator [12]. Therefore, in this Section we discuss methods for improving the bias and variance of the periodogram.

1) *Variance Reduction I*: A popular method for variance reduction in a periodogram is to average the periodogram estimate over several non-overlapping regions of the signal. This methodology was used, for example, in `ctffind3` [4] and `GCTF` [5]. Formally, we divide the signal into B non-overlapping blocks of size $K \times K$. The blocks are denoted by $\mathbf{y}_0, \dots, \mathbf{y}_{B-1}$. The power spectral densities (PSD) are estimated as the mean of all periodograms., i.e.

$$S_{AP}(u, v) = \frac{1}{B \cdot K^2} \sum_{b=0}^{B-1} \left| \sum_{k_1=0}^{K-1} \sum_{k_2=0}^{K-1} y_b[k_1, k_2] e^{-j2\pi(\frac{uk_1}{K} + \frac{vk_2}{K})} \right|^2, \quad (10)$$

$$A_{AP}(u, v) = \frac{1}{B \cdot K^2} \sum_{b=0}^{B-1} \left| \sum_{k_1=0}^{K-1} \sum_{k_2=0}^{K-1} y_b[k_1, k_2] e^{-j2\pi(\frac{uk_1}{K} + \frac{vk_2}{K})} \right|. \quad (11)$$

By averaging several estimates of the power spectrum, we reduce the variance of the estimation.

2) *Bias Reduction*: To understand the bias of the periodogram estimator, we consider a 1D, zero-mean, infinite stochastic signal \mathbf{z} . We would like to estimate the power spectrum of this signal. Unfortunately, only a portion of this signal is known. For simplicity, we define a new signal \mathbf{z}_K ,

$$\mathbf{z}_K[k] = \mathbf{z}[k] \mathbf{w}_K[k], \quad (12)$$

where \mathbf{w}_K is a 2D rectangular window,

$$\mathbf{w}_K[k] = \begin{cases} 1, & k = 0, \dots, K-1 \\ 0, & \text{otherwise} \end{cases}. \quad (13)$$

By (12) and the convolution theorem, the discrete Fourier transform (DFT) of \mathbf{z}_K is

$$\mathbf{Z}_K = \frac{1}{K} \mathbf{Z} \circledast \mathbf{W}_K, \quad (14)$$

where \mathbf{Z} is the true Fourier transform of \mathbf{z} , \mathbf{W}_K is the Fourier transform of the rectangular window \mathbf{w}_K , and \circledast is the circular convolution operator. The DFT of a rectangular window, \mathbf{W}_K , is known as the aliased sinc function,

$$\mathbf{W}_K(u) = \frac{\sin(K\pi u)}{\sin(\pi u)} \quad (15)$$

and is depicted in Figure 1(b).

Furthermore, the expectancy of S_P is a convolution between the true power spectral density function and the Fejér kernel [12]. The Fejér kernel,

$$\mathcal{F}_N(u) = \frac{\sin^2(K\pi u)}{K \sin^2(\pi u)} = \frac{1}{K} \sum_{t=0}^{K-1} \sum_{u=0}^{K-1} e^{j2\pi f(t-u)}, \quad (16)$$

is depicted in Figure 1(c).

The sidelobes of \mathbf{W}_K cause frequency leakage in the amplitude spectrum estimation, while the sidelobes of \mathcal{F}_N cause frequency leakage in the power spectrum estimation. This accounts for most of the bias of the periodogram estimator.

One method of lowering the bias of the periodogram estimation is tapering [12]. This method multiplies the data \mathbf{y} by a data taper, which is a window function possessing of smaller sidelobes than \mathbf{w}_K in its reciprocal space. The idea here is that smaller sidelobes lead to reduced frequency leakage. While many options for data tapers exist, Babadi

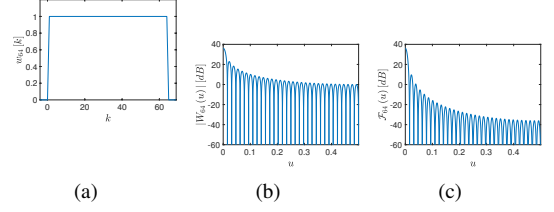


Fig. 1. Window effects. (a) Rectangular window w_K . (b) Example of $|W_K|$ for $K = 64$. (c) Example of Fejér's kernel for $K = 64$.

and Brown [9] suggest the use of the zeroth order discrete prolate spherical sequences (dpss) as data tapers.

The data taper can be applied to the entire micrograph. However, it is also possible to apply the data taper to each block of the micrograph, and average over the blocks to reduce variance. This idea was suggested by Welch [10]. In addition, Welch showed that a further variance reduction can be achieved when using overlapping blocks. Quite often, half-overlapping blocks are used [17], [18]. We therefore arrive at the modified periodogram,

$$S_{TP}(u, v) = \frac{1}{K^2} \left| \sum_{k_1=0}^{K-1} \sum_{k_2=0}^{K-1} y[k_1, k_2] w_{tp}[k_1, k_2] e^{-j2\pi(\frac{uk_1}{K} + \frac{vk_2}{K})} \right|^2, \quad (17)$$

$$A_{TP}(u, v) = \frac{1}{K^2} \left| \sum_{k_1=0}^{K-1} \sum_{k_2=0}^{K-1} y[k_1, k_2] w_{tp}[k_1, k_2] e^{-j2\pi(\frac{uk_1}{K} + \frac{vk_2}{K})} \right|^2, \quad (18)$$

where \mathbf{w}_{tp} denotes the 2D data taper.

3) *Variance Reduction II*: As mentioned in Section II-B1, averaging several periodogram estimates serves to lower the variance of the estimator. For this reason, Thompson [11] suggested that several tapers can be used. Each taper leads to a different estimate of the power or amplitude spectrum, and averaging over all these estimates will lead to reduced variance.

Combining all the above methods for variance and bias reduction, we arrive at the following estimator

$$S_{MT}(u, v) = \frac{1}{LBK^2} \sum_{b=0}^{B-1} \sum_{l=0}^{L-1} \left| \sum_{k_1=0}^{K-1} \sum_{k_2=0}^{K-1} y_b[k_1, k_2] w_{tp,l}[k_1, k_2] e^{-j2\pi(\frac{uk_1}{K} + \frac{vk_2}{K})} \right|^2, \quad (19)$$

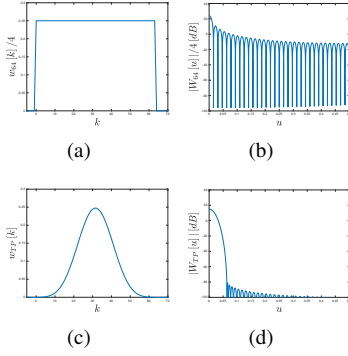


Fig. 2. Comparison between the rectangular window (top) and a data taper (bottom). On the left we compare the window in time. On the right we compare the sidelobes. Clearly, the data taper has lower sidelobes than the rectangular window.

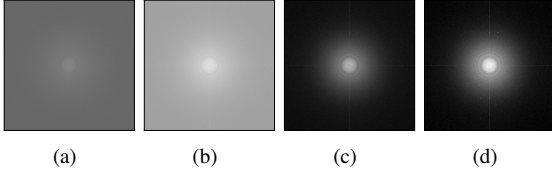


Fig. 3. Spectral density function estimation of a β -galactosidase micrograph from the EMPIAR-10017 dataset [1]. (a) Logarithm of periodogram estimation for micrograph. (b) Logarithm of average of periodogram over 512×512 blocks of the micrograph. (c) Logarithm of the data-taper estimation, averaged over 512×512 blocks of the micrograph and using single taper. (d) Logarithm of the multitaper estimation S_{TP} , also averaged over 512×512 blocks of the micrograph and 4 data tapers. We note that the ratio between the maximum and minimum values of the estimation is best for the multitaper estimation. For this reason the zero-crossings are easily identifiable.

$$A_{MT}(u, v) = \frac{1}{LBK^2} \sum_{b=0}^{B-1} \sum_{l=0}^{L-1} \left| \sum_{K-1=0}^{K-1} \sum_{k_2=0}^{K-1} y_b[k_1, k_2] w_{tp,l}[k_1, k_2] e^{-j2\pi\left(\frac{uk_1}{K} + \frac{vk_2}{K}\right)} \right|, \quad (20)$$

where $w_{tp,l}$ is the l th data taper, and y_b is the b th block of the micrograph.

Figure 3 presents a comparison between S_P , S_{AP} and S_{TP} . The smoothest method, depicted in the center column, is the multitaper estimation S_{TP} .

C. Background Subtraction

Analytically, the power spectrum we estimated in Section II-B can be expressed as the sum of two power spectra [2], [16],

$$P_A(u, v) = |H(u, v)|^2 PSD_x(u, v) + PSD_b(u, v), \quad (21)$$

where PSD_x is the power spectrum of the true particle projections and PSD_b is the power spectrum of noise, commonly referred to as background. In order to estimate the CTF parameters, many methods subtract the background from the PSD estimation of the micrograph [3], [2], to arrive at an estimation of the background subtracted power spectrum $|H(u, v)|^2 PSD_x(u, v)$.

The background is influenced by many factors. Creating a comprehensive model that takes into account all these factors is an open challenge. Instead, most background estimation methods treat the background as a well-behaved, monotonically decreasing function of spatial frequency [14]. This function is sometimes assumed to be radially symmetric, e.g. [2] where a Gaussian is fit to the minima of the 1D radial profile of the estimated power spectrum of the micrograph. The idea is that at spatial frequencies where the CTF has a zero crossing, the estimated power spectrum consists of the background alone. Other methods make no radial symmetry assumptions. An example of this approach is [3], where a low-pass filtered version of the estimated power spectrum is used for background estimation. In this manner, the background estimate is guaranteed to be smooth and decreasing.

In this paper, we suggest employing a linear program (LP) for background estimation. Following [2], we assume that the background is radially symmetric. We therefore consider the 1D radially symmetric averaged estimated power spectrum of the micrograph $S_{TP}(r)$, where $r = |g|$, and the 1D radial profile of the background $PSD_b(r)$.

The linear program we suggest minimizes the l_1 norm of the background subtracted power spectrum, subject to several linear constraints. The first of these is that the background subtracted power spectrum is non-negative. The second and third constraints ensure that the backgrounds is a well-behaved monotonically decreasing function,

$$\begin{aligned} & \text{minimize} \quad \sum_{r=1}^m S_{MT}(r) - PSD_b(r) \\ & \text{subject to} \quad PSD_b(r) < S_{MT}(r) \quad \forall r \\ & \quad \quad \quad PSD_b(r+1) < PSD_b(r) \quad \forall r \\ & \quad \quad \quad PSD_b(r+1) - 2PSD_b(r) + PSD_b(r-1) \geq 0 \quad \forall r. \end{aligned} \quad (22)$$

We present in Figure 4(a) the result of our LP background estimation method. We note that our method, unlike the methods presented above, ensures that the background subtracted power spectrum is non-negative. This can be seen in Figure 4(b).

After the 1D background has been estimated, we create a 2D radially symmetric background. To do this, we calculate

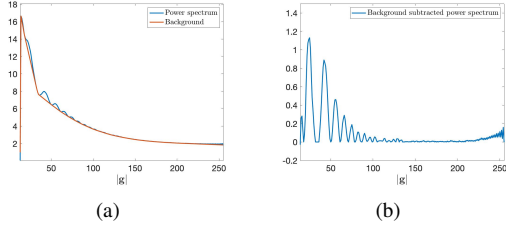


Fig. 4. Background estimation for a β -galactosidase micrograph from the EMPIAR-10017 dataset [1]. On the left is the 1D radial profile of the multi-taper power spectrum estimate S_{TP} and the estimated background $PSD_b(r)$. On the right is the background subtracted power spectrum.

the distance between each pixel and the center pixel, and assign its value accordingly. We denote the 2D background subtracted power spectrum as S_{MT}^- .

D. Denoising through Expansion over a Steerable Basis

In order to denoise the power spectrum, we consider the Taylor expansion of the CTF ?? around $\Delta f_1 - \Delta f_2 = 0$,

$$H(|\mathbf{g}|, \alpha_{\mathbf{g}}) = \sum_{n \text{ even}} (-1)^{\frac{n}{2}+1} \sin(\chi(|\mathbf{g}|, \alpha_{\mathbf{g}})) \left[\frac{1}{2} \pi \lambda (\Delta f_1 - \Delta f_2) \cos(2[\alpha_{\mathbf{g}} - \alpha_{ast}]) |\mathbf{g}|^2 \right]^n + \sum_{n \text{ odd}} (-1)^{\frac{n+1}{2}} \cos(\chi(|\mathbf{g}|, \alpha_{\mathbf{g}})) \left[\frac{1}{2} \pi \lambda (\Delta f_1 - \Delta f_2) \cos(2[\alpha_{\mathbf{g}} - \alpha_{ast}]) |\mathbf{g}|^2 \right]^n. \quad (23)$$

The first order expansion is

$$H(|\mathbf{g}|, \alpha_{\mathbf{g}}) = -\sin(\chi(|\mathbf{g}|, \alpha_{\mathbf{g}})) - \cos(\chi(|\mathbf{g}|, \alpha_{\mathbf{g}})) \left[\frac{1}{2} \pi \lambda (\Delta f_1 - \Delta f_2) \cos(2[\alpha_{\mathbf{g}} - \alpha_{ast}]) |\mathbf{g}|^2 \right] + R(|\mathbf{g}|, \alpha_{\mathbf{g}}), \quad (24)$$

where $R(|\mathbf{g}|, \alpha_{\mathbf{g}})$ is the remainder term. This term has a known bound of

$$R(|\mathbf{g}|, \alpha_{\mathbf{g}}) \leq \frac{1}{2} \left| \sin\left(\frac{1}{2} \pi \lambda (\Delta f_1 + \Delta f_2) |\mathbf{g}|^2 + \frac{1}{2} \pi \lambda c \cos(2[\alpha_{\mathbf{g}} - \alpha_{ast}]) |\mathbf{g}|^2 - \frac{1}{2} \pi \lambda^3 C_s |\mathbf{g}|^4 + w \right) \right| \leq \frac{1}{2} \left[\frac{1}{2} \pi \lambda (\Delta f_1 - \Delta f_2) \cos(2[\alpha_{\mathbf{g}} - \alpha_{ast}]) |\mathbf{g}|^2 \right]^2, \quad (25)$$

where $0 \leq c \leq \Delta f_1 - \Delta f_2$. The remainder term is negligible. To show this, we note that the electron wavelength λ is, according to the de Broglie relationship,

$$\lambda = \frac{h}{\sqrt{2meV}} = 12.25 \cdot 10^{-10} \frac{1}{\sqrt{V}}, \quad (26)$$

and V is typically $200 - 300 \text{ eV}$. Therefore, $\lambda < 10^{-10} \text{ m}$. In addition the astigmatism $(\Delta f_1 - \Delta f_2)$ is typically around $10^{-7} - 10^{-8} \text{ m}$. We see that $R(|\mathbf{g}|, \alpha_{\mathbf{g}})$ is bounded by $O(10^{-30})$.

We conclude that

$$H(|\mathbf{g}|, \alpha_{\mathbf{g}}) \approx -\sin(\chi(|\mathbf{g}|, \alpha_{\mathbf{g}})) - \cos(\chi(|\mathbf{g}|, \alpha_{\mathbf{g}})) \left[\frac{1}{2} \pi \lambda (\Delta f_1 - \Delta f_2) \cos(2[\alpha_{\mathbf{g}} - \alpha_{ast}]) |\mathbf{g}|^2 \right] \quad (27)$$

is a good approximation of the CTF. Using the identity

$$\cos(\alpha) = \frac{1}{2} e^{-j\alpha} + e^{-j\alpha},$$

we have

$$H(|\mathbf{g}|, \alpha_{\mathbf{g}}) \approx -\sin(A|\mathbf{g}|^2 + B|\mathbf{g}|^4 + w) - \frac{1}{4} \cos(A|\mathbf{g}|^2 + B|\mathbf{g}|^4 + w) D x |\mathbf{g}|^2 e^{j2(\alpha_{\mathbf{g}} - \alpha_{ast})} - \frac{1}{4} \cos(A|\mathbf{g}|^2 + B|\mathbf{g}|^4 + w) D x |\mathbf{g}|^2 e^{-j2(\alpha_{\mathbf{g}} - \alpha_{ast})}. \quad (28)$$

With a slight change in multiplication order

$$H(|\mathbf{g}|, \alpha_{\mathbf{g}}) \approx -\sin(A|\mathbf{g}|^2 + B|\mathbf{g}|^4 + w) - \cos(A|\mathbf{g}|^2 + B|\mathbf{g}|^4 + w) D e^{-j2\alpha_{ast} x} \left(\frac{|\mathbf{g}|}{2} \right)^2 e^{j2\alpha_{\mathbf{g}}} - \cos(A|\mathbf{g}|^2 + B|\mathbf{g}|^4 + w) D e^{j2\alpha_{ast} x} \left(\frac{|\mathbf{g}|}{2} \right)^2 e^{-j2\alpha_{\mathbf{g}}}. \quad (29)$$

On the other hand, the power spectrum of a micrograph is approximately compactly supported. This property is due to the exponential decay of the CTF envelope function. That is, the electron microscope does not only distort the projections through convolution with a point spread function, but also through convolution with a damping envelope, which suppresses the information in high frequencies [8].

Since the power spectrum is compactly supported, it can be expressed as a sum of Fourier-Bessel basis functions [19], [15] or as a sum of spherical Prolate wave functions [20]. In

this paper we focus on an expansion over the Fourier-Bessel basis,

$$\psi_{k,q}(|\mathbf{g}|, \alpha_{\mathbf{g}}) = \begin{cases} N_{kq} J_k(R_{kq}|\mathbf{g}|) e^{jk\alpha_{\mathbf{g}}}, & |\mathbf{g}| \leq 1 \\ 0 & \text{otherwise} \end{cases}, \quad (30)$$

where $\mathbf{g} = (|\mathbf{g}|, \alpha_{\mathbf{g}})$ is the polar coordinates of the spatial frequency \mathbf{g} , $\psi_{k,q}$ is the Fourier-Bessel basis function with radial frequency k and angular frequency q , J_k is the Bessel function of integer order k , defined as

$$J_k(r) = \sum_{v=0}^{\infty} \frac{(-1)^v (r/2)^{k+2v}}{v! (k+v)!} = \left(\frac{r}{2}\right)^k \sum_{v=0}^{\infty} \frac{(-1)^v (r/2)^{2v}}{v! (k+v)!}, \quad (31)$$

N_{kq} is a normalization factor and R_{kq} is the q th root of J_k .

The expansion of the power spectrum is then [19]

$$S_{MT}^{-}(|\mathbf{g}|, \alpha_{\mathbf{g}}) = \sum_{k=-\infty}^{\infty} \sum_{q=1}^{\infty} a_{k,q} \psi_{k,q}(|\mathbf{g}|, \alpha_{\mathbf{g}}), \quad (32)$$

where $a_{k,q}$ are the expansion coefficients computed as [19]

$$a_{k,q} = \int_0^c N_{kq} J_k\left(R_{kq} \frac{\eta}{c}\right) \eta d\eta \int_0^{2\pi} S_{MT}^{-}(\eta, \theta) e^{-jk\theta} d\theta. \quad (33)$$

Since the PSD is compactly supported, this infinite sum can be approximated by a finite sum,

$$\tilde{S}_{MT}^{-}(|\mathbf{g}|, \alpha_{\mathbf{g}}) = \sum_{k=-2L}^{2L} \sum_{q=1}^{p_k} a_{k,q} \psi_{k,q}(|\mathbf{g}|, \alpha_{\mathbf{g}}). \quad (34)$$

For convenience we define

$$M_{k,q} = a_{k,q} N_{kq} \sum_{v=0}^{\infty} \frac{(-1)^v (r/2)^{2v}}{v! (k+v)!}. \quad (35)$$

Therefore, (34) can be rewritten as

$$\tilde{S}_{MT}^{-}(|\mathbf{g}|, \alpha_{\mathbf{g}}) = \sum_{k=-2L}^{2L} \sum_{q=1}^{p_k} M_{k,q} \left(\frac{|\mathbf{g}|}{2}\right)^k e^{jk\alpha_{\mathbf{g}}}. \quad (36)$$

The number of angular frequencies p_k is determined by the maximal value of q such that $R_{kq} \leq \pi L$.

A comparison between (29) and (36) shows that we need only consider the radial frequencies $k = -2, 0, 2$. In fact, if we expand the CTF, or its square, over the Fourier-Bessel basis the coefficients of all odd valued radial frequencies (k) must be 0. This is also true for the expansion of $|H(|\mathbf{g}|)|^2 PSD_x(|\mathbf{g}|)$. If the amplitude or power spectrum of the micrograph has nonzero coefficients that correspond to odd valued radial frequencies, then this must be due to noise, and should be disregarded. Therefore, the projection onto the Fourier-Bessel basis has a denoising effect.

Therefore, the power spectrum we compute is

$$S(|\mathbf{g}|, \alpha_{\mathbf{g}}) = \sum_{q=1}^{p-2} a_{-2,q} \psi_{-2,q}(|\mathbf{g}|, \alpha_{\mathbf{g}}) + \sum_{q=1}^{p_0} a_{0,q} \psi_{0,q}(|\mathbf{g}|, \alpha_{\mathbf{g}}) + \sum_{q=1}^{p_2} a_{2,q} \psi_{2,q}(|\mathbf{g}|, \alpha_{\mathbf{g}}), \quad (37)$$

where $a_{-2,q}$, $a_{0,q}$ and $a_{2,q}$ are computed according to (33)

In Figure 5 we present the results of our PSD estimation method. We present the result of the multitaper PSD estimation as well as the result of the expansion of the background-subtracted power spectrum over the Fourier-Bessel basis. The result is smooth enough that many of the zero-crossings of the PSD can be easily resolved.

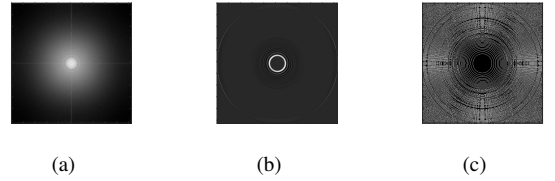


Fig. 5. .

E. CTF Estimation by Correlation

Under the assumption that PSD_x is constant in the relevant frequencies [2], [8], the background-subtracted power spectrum of the micrograph is proportional to the CTF squared. In addition, under this assumption, the background-subtracted amplitude spectrum is proportional to the CTF. For this reason, many approaches to CTF estimation use cross-correlation with simulated contrast transfer functions to estimate the parameters of the CTF [4], [3], [5].

Following the practice suggested in [5], we compute the cross correlation between the 1D rotational average of the background subtracted power spectrum and

$$H_{1D}(|\mathbf{g}|) = -\sin\left(\pi\lambda\Delta f_{1D}|\mathbf{g}|^2 - \frac{1}{2}\pi\lambda^3|\mathbf{g}|^4 + w\right). \quad (38)$$

The correlation function used is the Pearson correlation coefficient

$$P_{cc}(\Delta f_{1D}) = \frac{\sum_{r=1}^N |H_{1D}(r)| S_{avg}(r)}{\sqrt{\left(\sum_{r=1}^N H_{1D}(r)^2\right) \left(\sum_{r=1}^N S_{avg}(r)^2\right)}}, \quad (39)$$

where S_{avg} is the 1D radial profile of S (37). We create many simulated CTF functions, corresponding to a search over

the possible values of Δf_{1D} . Once the best value of Δf_{1D} is found, we run gradient descent the following correlation function

$$P_{cc}(\Delta f_1, \Delta f_2, \alpha_{ast}) = \frac{\sum_{\mathbf{g} < R} |H(|\mathbf{g}|, \alpha_{\mathbf{g}})| S(|\mathbf{g}|, \alpha_{\mathbf{g}})|}{\sqrt{\left(\sum_{\mathbf{g} < R} H(|\mathbf{g}|, \alpha_{\mathbf{g}})^2\right) \left(\sum_{\mathbf{g} < R} S(|\mathbf{g}|, \alpha_{\mathbf{g}})^2\right)}}, \quad (40)$$

where H is a simulated 2D CTF. This problem is initialized as in [5], where

$$\Delta f_1 = \Delta f_2 = \Delta f_{1D},$$

and α_{ast} is initialized from 6 values with a 30 degree separation between each two successive values.

An alternative method for initialization is through PCA. The moments of the power spectrum are computed and stored in a matrix \mathbf{M} ,

$$M_{1,1} = \sum_{g_x = g_y} g_x^2 \cdot S_{MT} \quad (41)$$

$$M_{1,2} = M_{2,1} = \sum_{g_x = g_y} g_x g_y \cdot S_{MT} \quad (42)$$

$$M_{2,2} = \sum_{g_x = g_y} g_y^2 \cdot S_{MT}, \quad (43)$$

The ratio between the eigenvalues of \mathbf{M} is the ratio between the two main directions in the image, which should approximately correspond to the major and minor axis of ellipses determined by the CTF. Therefore, the solution of the system

$$\Delta f_1 + \Delta f_2 = 2 * \Delta f_{1D}, \quad (44)$$

$$\frac{\Delta f_1}{\Delta f_2} = \frac{u_1}{u_2}, \quad (45)$$

where u_1, u_2 are the eigenvalues of \mathbf{M} , and $u_2 \leq u_1$.

F. CTF Estimation through Zero-Crossings

As the contrast transfer function can be expressed as a sine function, it reaches a zero when

$$\chi(\mathbf{g}, \Delta f, Cs, \lambda, w) = \pi m, \quad (46)$$

for any integer m . In Figure 5, we show the zero-crossing of the background-subtracted power spectrum. We note that these are closed, ellipse-like consecutive loops. We note that, for the set of spatial frequencies \mathbf{g}_l on a single loop,

$$\chi(\mathbf{g}_l, \Delta f, Cs, \lambda, w) = \pi m_l. \quad (47)$$

Furthermore, for the set of spatial frequencies \mathbf{g}_{l+1} on the following loop,

$$\chi(\mathbf{g}_{l+1}, \Delta f, Cs, \lambda, w) = \pi(m_l + 1). \quad (48)$$

We can therefore formulate a set of linear equations, where each equation corresponds to the spatial frequency of a pixel on a zero-crossings. Denote the set of pixels on three consecutive zero-crossing as $\mathbf{g}_l, \mathbf{g}_{l+1}, \mathbf{g}_{l+2}$, the system of equations will be

$$\begin{aligned} \frac{1}{2} \pi \lambda |\mathbf{g}_l|^2 (\Delta f_1 + \Delta f_2 - (\Delta f_1 - \Delta f_2)) \\ \cos(2[\alpha_{\mathbf{g}_l} - \alpha_{ast}]) - \frac{1}{2} \pi \lambda^3 |\mathbf{g}_l|^4 Cs + w = \pi m_l. \end{aligned} \quad (49)$$

$$\begin{aligned} \frac{1}{2} \pi \lambda |\mathbf{g}_{l+1}|^2 (\Delta f_1 + \Delta f_2 - (\Delta f_1 - \Delta f_2)) \\ \cos(2[\alpha_{\mathbf{g}_{l+1}} - \alpha_{ast}]) - \frac{1}{2} \pi \lambda^3 |\mathbf{g}_{l+1}|^4 Cs + w = \pi(m_l + 1). \end{aligned} \quad (50)$$

$$\begin{aligned} \frac{1}{2} \pi \lambda |\mathbf{g}_{l+2}|^2 (\Delta f_1 + \Delta f_2 - (\Delta f_1 - \Delta f_2)) \\ \cos(2[\alpha_{\mathbf{g}_{l+2}} - \alpha_{ast}]) - \frac{1}{2} \pi \lambda^3 |\mathbf{g}_{l+2}|^4 Cs + w = \pi(m_l + 2). \end{aligned} \quad (51)$$

The solution of this system will provide $\Delta f_1, \Delta f_2, \alpha_{ast}$ and m_l .

III. EXPERIMENTAL RESULTS

A. CTF Challenge

The CTF challenge [13] encompasses micrographs of 8 datasets of biological macromolecules and an additional dataset of synthetic micrographs. In this Section we compare the CTF estimation of our framework to the estimation provided by ctffind version 4.1.13 and Gctf. In order to compare the results, we compute the normalized cross-correlation (40) of each estimation with the amplitude spectrum of the micrograph. In order to keep from biasing the results towards a specific framework, we compute the amplitude spectrum according to 11.

The first dataset consists of 16 micrographs of GroEL. The micrographs were acquired by A. Cheng using Tecnai F20 microscope operating at 200 kV and a TVIPS F415 camera. The pixel size corresponds to 1.34 Å per pixel. Spherical aberration was 2 mm and amplitude contrast was considered 0.07.

The second dataset was recorded using a DE-12 direct detector. All other parameters are the same as reported for the first dataset.

The third and fourth datasets were not included in our experiment. The reason for this is that these datasets were collected in over-saturated conditions. This causes the background of the PSD to increase in high frequencies [21]. As our background estimation framework enforces a decrease of background towards the high frequencies, under over-saturated conditions our background estimation will produce bad results.

The fifth dataset was provided by R. Henderson and S. Chen. This dataset contains 17 micrographs of Apoferritin, collected using a Polara microscope operating at 200 kV and recorded on film. The pixel size corresponds to 1.63 Å per pixel. Spherical aberration was 2 mm and amplitude contrast was considered 0.05.

The sixth dataset was provided by W. Chiu and J. Jakana. This dataset contains 17 micrographs of Apoferritin, collected using a EM3200FSC microscope operating at 300 kV and recorded using a DE-12 direct detector. The pixel size corresponds to 1.18 Å per pixel. Spherical aberration was 4.1 mm and amplitude contrast was considered 0.1.

The last two datasets contain micrographs of TMV virus. The seventh dataset contains 24 micrographs collected using a CM200 FEG microscope operating at 200 kV and TVIPS F416 CMOS camera. The pixel size corresponds to 2.19 Å per pixel. Spherical aberration was 2.26 mm and amplitude contrast was considered 0.07. The eighth dataset is the noisiest, and therefore most challenging, dataset. It contains 34 micrograph collected using a Polara microscope operating at 300 kV and a TVIPS F416 CMOS camera. The pixel size corresponds to 1.18 Å per pixel. Spherical aberration was 2 mm and amplitude contrast was considered 0.07.

B. Consistency in low SNR

To test consistency of results with changing SNR, we estimate CTF parameters from a sum of motion-corrected frames. We change the number of frames in each sum and compare results as the number of frames, and thus the SNR, decreases. For this experiment we use a micrograph of the EMPIAR-10252 dataset. This is a dataset of Catalytic subunit of protein kinase A bound to ATP, manganese, and IP20.

ACKNOWLEDGEMENT

This work has made use of electron micrographs provided by the following researchers: Richard Henderson (Medical Research Council, UK), Henning Stahlberg (University of Basel), Joachim Frank (Columbia University), Wah Chiu (Baylor College of Medicine), An-chi Cheng (Scripps Research Institute), as well as resources from the Biocomputing Unit of the Spanish National Center for Biotechnology

(CNB-CSIC) as part of an ESFRI Instruct support project from the Ministry of Economy and Competitiveness (AIC-A-2011-0638)

REFERENCES

- [1] U. Valdré, *Electron Microscopy in Material Science*. Academic Press, 1971, ch. Phase Contrast Electron Microscopy by F. Thon.
- [2] J. Zhu, P. A. Penczek, R. Schröder, and J. Frank, "Three-Dimensional reconstruction with contrast transfer function correction from energy-filtered cryoelectron micrographs: Procedure and application to the 70S *Escherichia coli* Ribosome," *Journal of Structural Biology*, vol. 118, no. 3, pp. 197 – 219, 1997.
- [3] A. Rohou and N. Grigorieff, "CTFFIND4: Fast and accurate defocus estimation from electron micrographs," *Journal of Structural Biology*, vol. 192, no. 2, pp. 216–221, 2015.
- [4] J. A. Mindell and N. Grigorieff, "Accurate determination of local defocus and specimen tilt in electron microscopy," *Journal of Structural Biology*, vol. 142, no. 3, pp. 334–347, June 2003.
- [5] K. Zhang, "Gctf: Real-time CTF determination and correction," *Journal of Structural Biology*, vol. 193, no. 1, pp. 1–12, 2016.
- [6] K. Tani, H. Sasab, and C. Toyoshima, "A set of computer programs for determining defocus and astigmatism in electron images," *Ultramicroscopy*, vol. 65, pp. 31–44, 1996.
- [7] R. Yan, K. Li, and W. Jiang, "Real-time detection and single-pass minimization of tem objective lens astigmatism," *Journal of Structural Biology*, vol. 197, no. 3, pp. 210 – 219, 2017.
- [8] C. Sorzano, S. Jonic, R. Nez-Ramrez, N. Boisset, and J. Carazo, "Fast, robust, and accurate determination of transmission electron microscopy contrast transfer function," *Journal of Structural Biology*, vol. 160, no. 2, pp. 249–262, 2007.
- [9] B. Babadi and E. N. Brown, "A review of multitaper spectral analysis," *IEEE Transactions on Biomedical Engineering*, vol. 61, no. 5, pp. 1555–1564, May 2014.
- [10] P. D. Welch, "The use of fast fourier transform for the estimation of power spectra: A method based on time averaging over short, modified periodograms," *IEEE transactions on audio and electroacoustics*, vol. 15, no. 2, pp. 70–73, 1967.
- [11] D. J. Thomson, "Spectrum estimation and harmonic analysis," *Proceedings of the IEEE*, vol. 70, no. 9, pp. 1055–1096, Sep. 1982.
- [12] D. B. Percival and A. T. Walden, *Spectral Analysis for Physical Applications multitaper and conventional univariate techniques*. Cambridge University Press, 1993.
- [13] R. Marabini, B. Carragher, S. Cheni, J. Chen, A. Cheng, K. H. Downing, J. Frank, R. A. Grassucci, J. B. Heymann, W. Jiang, S. J. Hstau Y. Liao, S. J. Ludtke, S. Patwari, A. L. Piotrowski, A. Quintana, C. O. Sorzano, H. Stahlberg, J. Vargas, N. R. Voss, W. Chiu, and J. M. Carazo, "CTF Challenge: Result summary," *Journal of Structural Biology*, vol. 190, no. 3, pp. 348–359, Juen 2015.
- [14] J. Frank, *Three-Dimensional Electron Microscopy of Macromolecular Assemblies*. Academic Press, 1996, ch. 2 (Electron Microscopy of Macromolecular Assemblies), pp. 12–53.
- [15] T. Bhamre, Z. Zhao, and A. Singer, "Mahalanobis distance for class averaging of cryo-em images," in *2017 IEEE 14th International Symposium on Biomedical Imaging (ISBI 2017)*, April 2017, pp. 654–658.
- [16] A. Saad, S. J. Ludtke, J. Jakana, F. J. Rixon, H. Tsuruta, and W. Chiu, "Fourier amplitude decay of electron cryomicroscopic images of single particles and effects on structure determination," *Journal of Structural Biology*, vol. 133, no. 1, pp. 32 – 42, 2001.
- [17] J. J. Fernández, J. R. Sanjurjo, and J.-M. Carazo, "A spectral estimation approach to contrast transfer function detection in electron microscopy," *Ultramicroscopy*, vol. 68, no. 4, pp. 267 – 295, 1997.

- [18] Z. Huang, P. R. Baldwin, S. Mullapudi, and P. A. Penczek, "Automated determination of parameters describing power spectra of micrograph images in electron microscopy," *Journal of Structural Biology*, vol. 144, pp. 79 – 94, 2003.
- [19] Z. Zhao, Y. Shkolnisky, and A. Singer, "Fast steerable principal component analysis," *IEEE Transactions on Computational Imaging*, vol. 2, no. 1, pp. 1–12, 2016.
- [20] B. Landa and Y. Shkolnisky, "Steerable Principal Components for Space-Frequency Localized Images," *SIAM Journal on Imaging Sciences*, vol. 10, no. 2, pp. 508–534, 2018.
- [21] X. Li, S. Q. Zheng, K. Egami, D. A. Agard, and Y. Cheng, "Influence of electron dose rate on electron counting images recorded with the k2 camera," *Journal of Structural Biology*, vol. 184, no. 2, pp. 251 – 260, 2013.